Contrib Mineral Petrol (2003) 146: 263–274
DOI 10.1007/s00410-003-0498-2

ORIGINAL PAPER

**Thomas H. K. Lohkämper · Guntram Jordan
Raoul Costamagna · Bernhard Stöckhert
Wolfgang W. Schmahl**

Phase shift interference microscope study of dissolution-precipitation processes of nonhydrostatically stressed halite crystals in solution

Received: 6 June 2002 / Accepted: 13 June 2003 / Published online: 15 August 2003

Abstract Halite single crystals in saturated solution were used to study dissolution precipitation creep (DPC) at conditions where plastic deformation is negligible. Specifically, the free unloaded surfaces of these crystals were investigated by a novel Linnik-based phase shift interference microscope. The method allows observations of the crystal surface in-situ and with an axial resolution in the nanometer scale. Transport phenomena in open systems, temperature gradients, and gradients in strain energy density were found to cause morphological changes on the free crystal surface by dissolution/reprecipitation. We did not find evidence for DPC by applying a homogeneous stress field to the crystal as long as plastic deformation was avoided. These findings suggest that deformation of rocks by DPC in situations where dislocation creep is not activated, but is rather promoted by fluid transport through the rock or by episodic changes of extensive parameters affecting solubility than by homogeneous stress alone.

Introduction

Since Sorby (1863a, 1863b, 1865), dissolution precipitation creep (DPC) or pressure solution is considered to be the predominant mechanism of sediment compaction and an important deformation mechanism during low to intermediate grade metamorphism at stresses insufficient to activate dislocation creep (e.g., Rutter 1976; McClay 1977), as shown by the microstructural record of metamorphic rocks (e.g., Elliott 1973; Rutter 1983; Groshong 1988; Knipe 1989; Schwarz and Stöckhert 1996; Stöckhert et al. 1999). DPC may also play a considerable role in the rheological behaviour of rocks containing partial melts (Hirth and Kohlstedt 1995; Rosenberg 2001). Based on Gibbs' (1906) consideration of the thermodynamics of nonhydrostatically stressed solid bodies, many authors have suggested theoretical treatments of DPC (Weyl 1959; Kamb 1961; Paterson 1973; Rutter 1976; Lehner and Bataille 1984/85; Lehner 1990, 1995; Leroy and Heidug 1994; Heidug 1995). The common idea is that the deviatoric stress on solids should drive deformation via a dissolution-precipitation mechanism, i.e., dissolution at the loaded grain-to-grain contact, and diffusional transport out of the contact zone to the adjacent grain boundaries which are perpendicular to the extensional component of the deviatoric stress tensor, where the material is supposed to reprecipitate (e.g., Paterson 1973; McClay 1977; Shimizu 1995). This process is also described as a "convergence" of the compressionally stressed counter-surfaces, while the grain elongates in the perpendicular direction (Heald 1956; Durney 1976). Lehner and Bataille (1984/85) and Lehner (1990, 1995) pointed out that such a scenario is not likely to be appropriately described by concepts of reversible processes, and discussed DPC in terms of nonequilibrium thermodynamics, solute supersaturation, and transport conditions. Another mechanism assumed to drive DPC has been suggested by Ostapenko (1968) who supposed that the "contacts between compressed grains become zones of microgranulation composed of minute crystalline grains". Recently, Bos et al. (2000) have presented the microstructural results of rotary shear experiments on brine-saturated mixtures of halite and kaolinite. They attributed the observed frictional-viscous behaviour to the combined effects of pressure solution and sliding along kaolinite-rich foliation planes. Based on these experiments, Bos and Spiers (2002)

Editorial responsibility: J. Hoefs

T. H. K. Lohkämper · G. Jordan · B. Stöckhert
W. W. Schmahl (✉)
Institut für Geologie, Mineralogie und Geophysik,
Ruhr-Universität Bochum,
44780 Bochum, Germany
E-mail: Wolfgang.Schmahl@ruhr-uni-bochum.de
Tel.: +49-023-43224381
Fax: +49-023-43214433

R. Costamagna
Institut für Mechanik, Ruhr-Universität Bochum,
44780 Bochum, Germany

developed a "microphysical" model, which described the experimental data on the halite-kaolinite system reasonably well. Den Brok and Morel (2001) addressed the role of the elastic strain energy, although it is often assumed not to play a major role in DPC processes.

Apart from micromechanisms, the structure of the liquid layer separating grains in a solid undergoing DPC is still a matter of debate. While some authors invoked a continuous fluid film (Weyl 1959; Rutter 1983; Derjaguin et al. 1987; Hickman and Evans 1991; Heidug 1995), others expected, and in some cases were able to demonstrate, an interface structure consisting of fluid pockets and channels separated by load-bearing islands displaying a dynamically stable island and channel structure (Raj and Chyung 1981; Urai et al. 1986; Spiers and Schutjens 1990; Lehner 1995). Leroy and Heidug (1994) presented a theory of surface roughness in fluid-filled tubular pores assuming perturbations and interface-controlled kinetics.

Experimental studies can be subdivided into two groups: (*i*) Compaction or deformation experiments on granular aggregates (e.g., Urai et al. 1986; Spiers and Schutjens 1990; Spiers et al. 1990; Spiers and Brzesowsky 1993; de Meer and Spiers 1997; den Brok et al. 1999a, 1999b; Bos et al. 2000; Renard et al. 2000, 2001), and (*ii*) experiments on single crystals (e.g., Tada and Siever 1986; Hickman and Evans 1991, 1995; Gratier 1993; Röller et al. 1995; Martin et al. 1999; Schutjens and Spiers 1999; Morel and den Brok 2001; de Meer et al. 2002). All these experiments done on analogue model systems showed that fluid can affect the rheological behaviour of rocks.

The present study is focussed on in-situ observations of changes in the fine-scale morphology of free surfaces of single crystals when stress is imposed. The effect of stress on this surface is then compared to other factors controlling dissolution or growth. The idea is to use the processes observed at the free surface as a proxy for the expected dissolution at the loaded interface of the single crystal. Based on single crystal experiments, various authors have reported widely varying convergence rates. Hickman and Evans (1991, 1995) conducted experiments with calotte-shaped crystals in contact with planar surfaces. Their observed convergence rates for loads up to 14 MPa at halite-silica contacts reached 10–50 nm/day. In halite-halite experiments no convergence was observed. The absence of convergence was explained by "neck growth" driven by gradients in surface curvature provided that the wetting angle between the two solids is non-zero (Hickman and Evans 1991). In contrast, Martin et al. (1999) exposed mm-sized halite crystals in contact with muscovite, quartz or halite to a homogeneous load ≤ 2 MPa and obtained convergence rates of 0.1–2 μm/day independent of the nature of the interface. Tada and Siever (1986) created plastically deformed zones at the contact of an indenter and its periphery. These zones dissolved in a solution saturated with respect to the unperturbed solid and thus contributed to DPC by a combination of plastic deformation at the contact and free surface pressure dissolution in the periphery of the indenter. Recently, de Meer et al. (2002) reported widening of loaded annular contacts, which they observed by conventional optical microscopy.

In order to resolve the contributions of various parameters to DPC, we used a new optical interference microscope based on the phase-shifting technique (Bruning et al. 1974) to observe crystals undergoing DPC in different stress states in-situ. For the study of crystal growth and dissolution with unit-cell resolution, atomic force microscopy (AFM) has become the most popular in-situ method (e.g., Astilleros et al. 2000; Jordan et al. 2001; Teng et al. 2001; Jones et al. 2003; Peskleway et al. 2003). AFM, however, requires close-distance interaction between the AFM probe and the sample surface. Therefore, its non-invasive capabilities are limited, and it utilises a complex setup to scan the tip with respect to the surface. In contrast to AFM, the interference microscope unites true non-contact imaging and high axial resolution by recording a series of reflected light interferograms from a surface that is shifted axially with respect to a reference mirror by a piezo actuator. Comparison of the phase-shifted interferograms allows a three-dimensional reconstruction of the surface topography with nm resolution in the axial direction and conventional optical resolution in the lateral dimensions. Onuma et al. (1993, 1994) introduced the phase shift technique to the study of crystal growth processes using laser light. Commercial white-light and phase-shift interferometers are widely used in semiconductor and other industries requiring high-resolution surface characterisation (Sandoz 1996; Hart et al. 1998; Aziz 1998). These interferometric techniques have been introduced to earth sciences by MacInnis and Brantley (1993) and Lüttge et al. (1999, 2003) for ex-situ studies of mineral dissolution processes. However, the available instruments mainly use Mirau-interferometers, which makes it practically impossible to compensate changes in optical path-lengths between the objective lens and the object. In in-situ experiments, such changes are unavoidably caused by the fluid layer on the sample surface. Therefore we resolved to use the interferometer setup designed by Linnik (1933).

Experimental

Linnik type phase shift interference microscope (PSIM)

In co-operation with ATOS GmbH (Germany), a Linnik type phase shift interference microscope was constructed (Fig. 1). In contrast to a Michelson or Mirau interferometer the Linnik interferometer splits the beam into a sample-beam path and a reference-beam path, each beam path equipped with a separate objective lens (Linnik 1933). Any material (e.g., fluids, cover-windows) between the sample surface and the lens causes an optical retardation in the sample-beam path with respect to the reference-beam path. The PSIM compensates this retardation by extending the length of the reference-beam path (Fig. 1, left side) or by inserting similar materials between the reference mirror and the reference lens. With commercially available instruments like a Mirau interferometer (e.g., Mirau 1955) the compensation is not possible, unless laser light is used. However, the long coherence length of laser light

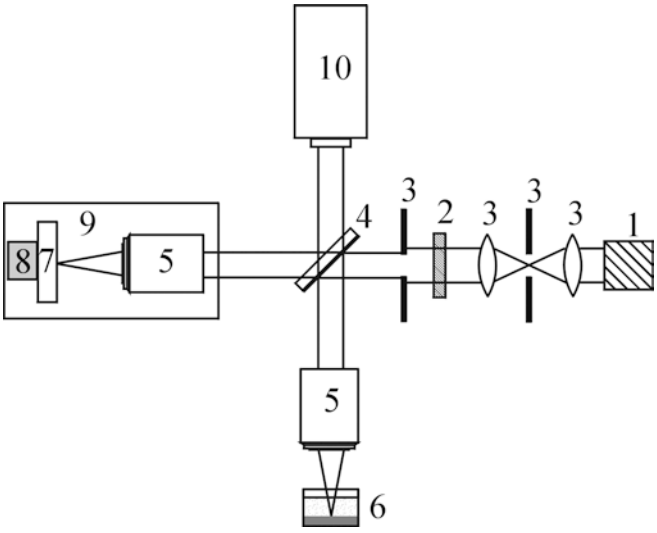

Fig. 1 Schematic drawing of the phase shift interference microscope (PSIM) based on the Linnik-principle with two coupled lenses. Topographic analysis of crystal-fluid interfaces through liquid and glass covers is possible. *1* Light source, *2* monochromatic filter, *3* lens and aperture system, *4* beam splitter, *5* 50× lenses, *6* sample surface covered with glass and fluid layer, *7* moveable reference mirror, *8* piezo actuator, *9* Linnik compensation (moveable), *10* CCD camera

causes highly disturbing interferences from lateral scattering speckles and from all reflecting surfaces in the beam path. The PSIM applies light from a light bulb monochromatized by a filter [$\lambda = (555 \pm 25)$ nm]. The acquisition of a series of interferograms is performed by scanning the optical path length between the sample surface (or the reference surface) and the beam splitter by a piezo actuator in regular steps of a wavelength. The morphology of the sample is calculated subsequently from the shift of the interference fringes in these consecutive interferograms. The image acquisition and the calculation only needs a few seconds. The lateral resolution of the apparatus (with 50× lenses and the wave length used) is approximately 0.6 μm. The maximum field of view is 166×124 μm^2.

Sample preparation and sample cell

In order to study growth or dissolution on the free surface of a crystal subject to uniaxial stress, a cell was constructed in which the axis of compressive stress is perpendicular to the direction of view of the PSIM. The cell is schematically shown in Fig. 2. The inner volume of the cell is approx. 700 mm^3; the cell and piston were made of passivated titanium and are embedded in a copper block thermostated by Peltier elements. The diameter of the SiO_2 glass cover is 20 mm and the thickness is 0.5 mm. The temperature is controlled via two Pt-100 thermosensors, one mounted near a Peltier element, the other 200 μm apart from the sample within the cell wall. In all experiments, the temperature was (30 ± 0.05) °C. An infrared camera did not show any lateral temperature gradient in the cell; thermocouple measurements inside the cell revealed a vertical temperature gradient of 0.006 to 0.01 K/mm. The cell can be operated in two different modes representing either a closed or a quasi-open system. The closed system was achieved by an O-ring seal and additional sealing with viscous silicone around the glass cover. This seal cannot and need not resist increasing hydrostatic pressures in the cell. In the closed system an applied stress of 0.5 MPa causes the piston to advance by 4 mm into the fluid-filled cell without crystal. The increased hydrostatic pressure causes the glass cover to bulge slightly. In the actual experiments the intrusion of the piston was only a few microns, so that in fact the increase in hydrostatic pressure in the cell is insignificant. The

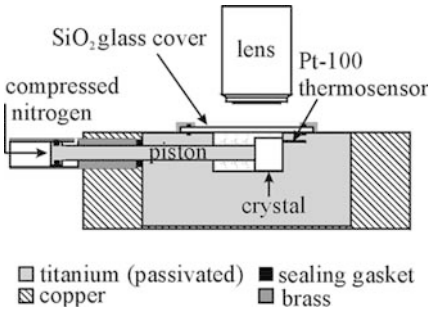

Fig. 2 Sketch of the cell. The piston of the cell is loaded with compressed nitrogen and can support pressure of up to 100 MPa depending on the geometry and size of the crystal. The outer diameter of the titanium cell is 30 mm and the diameter of the piston is 3 mm

quasi-open system was achieved by not perfectly tightening the window O-ring seal without any additional sealing and therefore creating a capillary-like exit.

Synthetic (Korth Kristall, Germany; Young's modulus = 39.98 GPa) and natural (unknown origin) halite crystals were used. X-ray diffraction and energy-dispersive X-ray spectrometer (EDX) revealed similar structure and chemical composition for both kinds of crystals. Judging by dissolution etch pit density, the dislocation density was ca. 3.6×10^6 m^{-2} for the artificial crystal and ca. 4.4×10^6 m^{-2} for the natural crystal and therefore rather similar. The crystals were cleaved with a scalpel parallel to (100) immediately before mounting them into the cell (max. size 5×6×4.7 mm^3). For the preparation of saturated NaCl-solution reagent-grade NaCl (Baker, Netherlands) and deionized water (18 MΩ cm) were used.

Stress was applied to the crystal via a piston loaded with compressed nitrogen. Different pistons were used to apply different stress states A, B and C (Fig. 3). The stress states A and B are used to introduce gradients in elastic strain energy density. The distribution of elastic strain energy density is calculated by finite elements method (FEM). In the case of a cylindrical piston (stress state A), the elastic strain energy density is the highest at the contact area. At the unloaded surfaces, the elastic strain energy density is smallest in the region close to the piston and higher in the opposite region. If a rectangular piston is pressed at the crystal in a way that one side of the piston extends beyond the crystal surface (stress state B), the elastic strain energy density on the free surface is highest close to the piston and less in the opposite region close to the cell wall. In contrast to the inhomogeneous stress states A and B, stress state C represents a near homogeneous distribution of elastic strain energy density. In all three stress states, friction occurs along the contacts in the same order of magnitude. Our comparative FEM calculations confirm that in all three stress states friction causes negligible gradients in elastic strain energy density at the free surface compared to the gradients caused by piston geometry in the cases A and B. The values of the applied stress given here refer to the force exerted by the nitrogen divided by the nominal contact area between (1) piston and crystal and (2) crystal and the counter bearing cell wall. In the stress states A and B, the crystal-cell wall contact area was larger than the piston-crystal contact area causing less stress at the crystal to cell wall contact area. In the experiments, the stress at the crystal to cell wall contact was limited to ≤ 1 MPa (Table 1) and, therefore, can be assumed to be below the elastic limit of halite which is in air between 0.85 and 1.5 MPa (Wimmer et al. 1963). In experiments according to stress states A and B, piston and cell wall were made of passivated titanium (surface roughness $R_a \sim 0.5$ μm characterized by PSIM, R_a is the average distance of the data points from the mean plane). For the stress state C, two SiO_2 glass plates with $R_a \leq 1$ nm were used. However, we note that asperities and steps on the (100) halite surface can cause local contacts, where the load can exceed the threshold for plastic deformation.

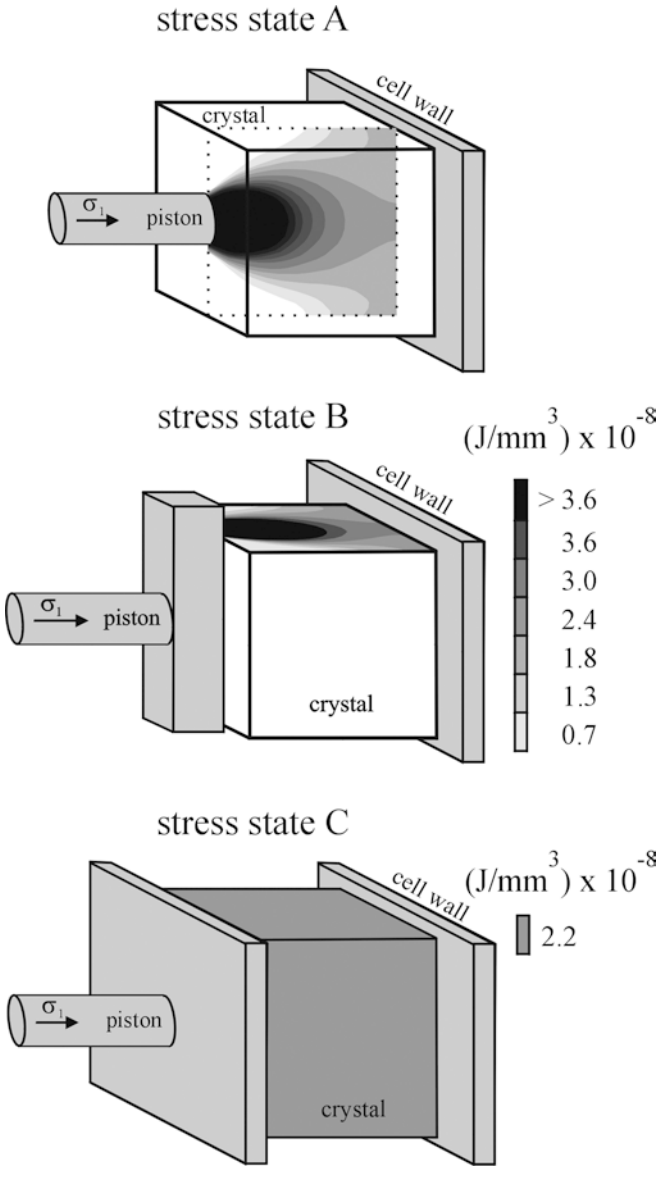

Fig. 3 Experimental setups for creating different kinds of stresses. Cylindrical piston for inhomogeneous stress (stress state *A*), rectangular piston for inhomogeneous stress, where the highest amount of elastic strain energy is below the piston and on the surface near the piston (stress state *B*) and rectangular pistons for producing a nearly homogeneous state of stress in the crystal (stress state *C*). The distribution of elastic strain energy density in a halite crystal is calculated by finite elements method for all three stress states and is shown qualitatively for the stress state A in y-z cross section and quantitatively for the stress states *B* and *C* (in x-y cross section). The calculations are based on a linear elastic and isotropic case without friction at 1 MPa at the contact crystal-cell wall with elastic $\text{modulus}_{\text{halite}} = 23$ GPa and Poisson's ratio $\nu = 0.16$

Results

Surface morphology induced by adding solution to the crystal

The typical morphology of a freshly cleaved halite (100) surface in air is shown in Fig. 4a. The surface consists of

Table 1 Experimental conditions and results. The nominal size of the contact area is $w \times h$

Experiment	Closed systems					Quasi-open systems		
	E 1	E 2	E 3	E 4.1	E 4.2	E 5	E 6	E 7
Duration (days)	0.5	8	30	17	17	8	28	8
Crystal[a]	s	s	s	s		n	n	n
Size of crystal (mm) ($w \times l \times h$)	5×6×4.7	5×1×4	5.8×2.8×3	3.9×4.1×5		5×5×3	3.3×3×1.8	5×5×4
Stress state	–	A	B	–	A	C	A	A
Added solution saturated at (°C)	22	~35	30	30		30	21.5	21.8
Temperature of crystal before adding solution (°C)	22	30	30	30		30	21.5	21.8
Temperature in experiment (°C)	30	30/RT	30	30		30	30	30
Stress applied at piston-crystal (MPa)	–	0.5	1.9	0	2.2	0.3	1.3/0.65/0.32/0.13	1
Stress applied at crystal-cell wall (MPa)	–	0.2	0.3	0	1	0.3	1/0.5/0.3/0.1	0.4
Observations	Increased roughness/retreat of rim	(No) migration f steps	Dissolution on surface	Migration of steps	Retreat of rim (100 nm/day)	No retreat of rim	Retreat of rim (2.5 μm/day)	Retreat of rim (13.5 μm/day)

[a] *n* Natural crystal; *s* Synthetic crystal; stress state (see Fig. 3); *RT* room temperature; *w* width, *l* length, *h* height

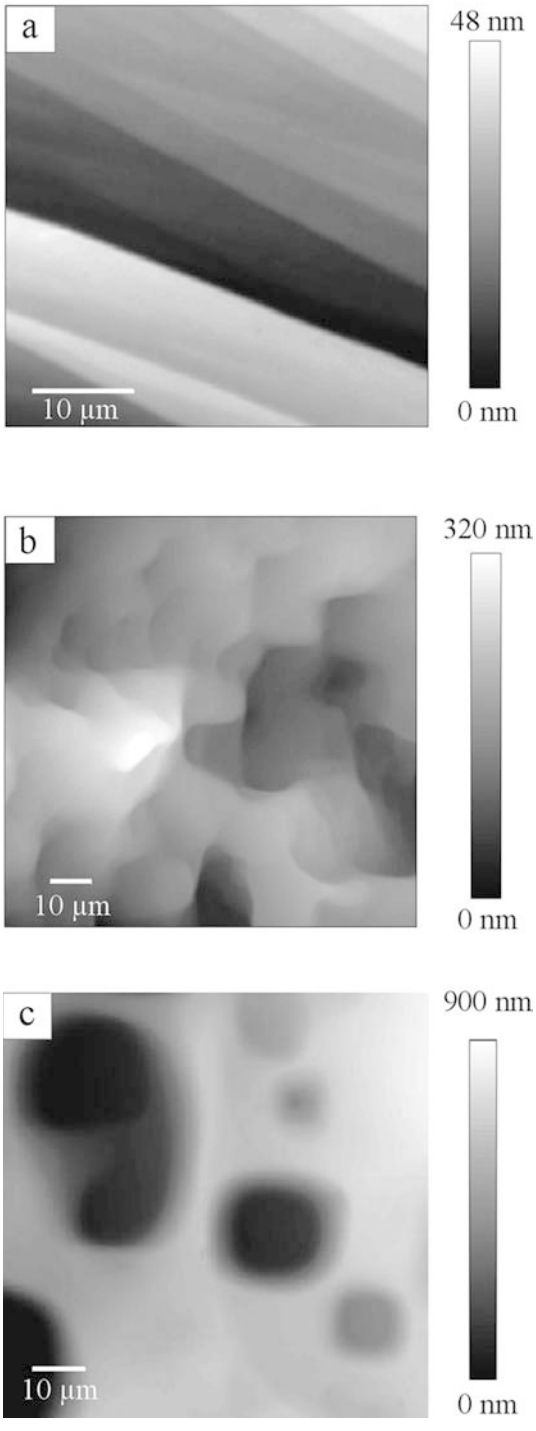

Fig. 4 a Typical topography of a freshly cleaved (100) halite surface measured in air by PSIM. **b** Halite (100) surface at 30 °C after preheated (approx. 29–30 °C), saturated NaCl-solution has been added. The image was acquired in-situ through a glass cover and saturated solution. **c** In-situ measurement of halite (100) surface; surface roughening and etch pits were caused by heating-up from room temperature to 30 °C

smooth terraces and cleavage steps of up to few tens of nm in height; larger cleavage steps were infrequent. The average roughness of the surface shown in Fig. 4a is $R_a = 9.5$ nm. After the crystals had been mounted into the cell, the dry cell was heated up to (30 ± 0.05) °C. Then, preheated (approx. 29–30 °C), saturated NaCl-solution was added. Figure 4b shows the characteristic surface topography after the solution had been added. The surface morphology extensively changes until all parts of the system have equilibrated. An equilibrium in the strict sense cannot be reached due to the small thermal gradients (see below). At this stage, the roughness increased to $R_a \sim 43$ nm. In accordance to the cell dimensions and the diffusion velocity of Na^+ and Cl^-, this quasi-equilibrium was reached within a few hours in the closed system (experiments E 3, E 4.1, E 5; see Table 1).

If the cell was loaded with the crystal and the solution together at room temperature and subsequently heated up to 30 °C (experiments E 1, E 6, E 7; see Table 1), dissolution preferentially took place on the surface by the development of etch pits and by dissolution at crystal edges (Fig. 4c). In this case the average roughness of the surface was $R_a \sim 145$ nm. The depth of the etch pits reached up to 600 nm.

Quasi-equilibrium without applied stress (closed system)

After the quasi-equilibrium between the crystal and the solution was achieved at 30 °C, the halite crystals showed growth at the surface facing the optical window (Fig. 5a and b; experiments E 2, E 4.1; see Table 1). The preferential deposition of material occurred at surface steps with a height of one to two microns. The step velocities varied between (7.2 ± 3) and (84 ± 3) µm/day. Other steps, even close to these advancing steps, showed neither growth nor dissolution within the resolution limits of PSIM (Fig. 5c and d). In experiment E 2 the temperature was reduced from 30 °C to room temperature. The resulting supersaturation led to an increase in step growth of up to 200 µm/day within the next few hours. After a new quasi-equilibrium was attained at room temperature, the steps were observed during 5 hours, while room temperature varied between 21.9 and 22.0 °C within this time period. At the level of accuracy achieved by the optical measurement, there was no evidence for step movement on the entire surface.

Surface morphology induced by applied stress (closed system)

In experiment E 4.2, stress was applied to the crystal (Fig. 3, stress state A), but did not lead to significant changes in the advance of steps observed in the quasi-equilibrium state. In Fig. 6, step movement is plotted versus time. For the data points taken in the stress-free quasi-equilibrium state (exp. E 4.1) open symbols are used, while data points in the stressed state (exp. E 4.2) are marked with closed symbols. The application of stress did not significantly enhance the step advance. The average step velocity even decreased slightly. The immobile steps

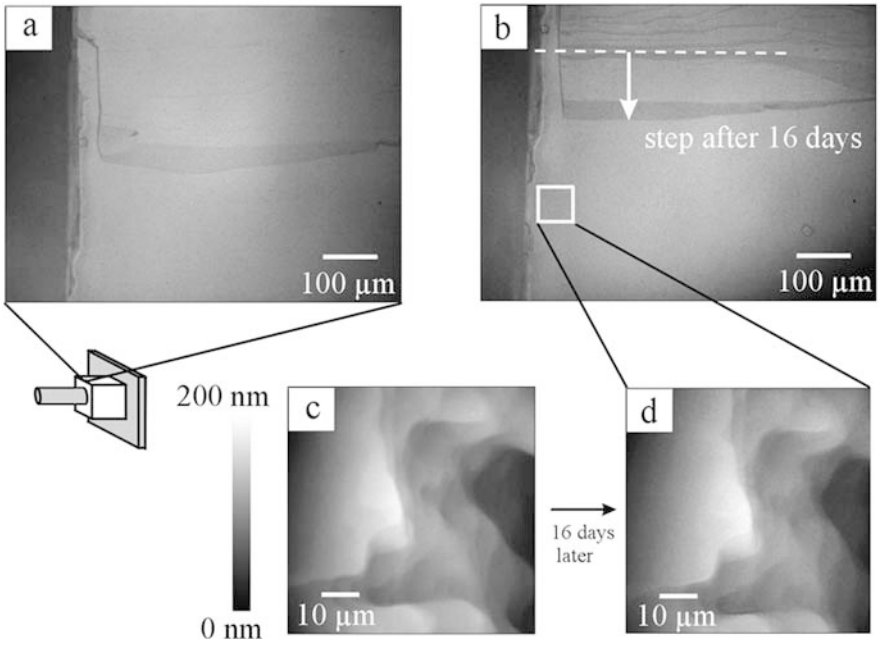

Fig. 5 The images **a** and **b** (reflected optical micrographs, grey scales do not represent surface heights) show a macroscopic step with a step growth velocity of approx. 8 µm/day and a height of 1–2 µm. The *dashed line* in **b** indicates the former step position in image **a**. Despite the growth at this step, no growth or dissolution could be seen at locations close to this advancing step within the resolution limits of PSIM (images **c** and **d**)

observed in the quasi-equilibrium state remained immobile while stress was applied to the crystal.

In order to investigate the expected convergence of the compressionally stressed counter-surfaces of the crystal, we observed the edge of the free surface facing the cell wall. As shown in Fig. 3, stress state A, possible dissolution at the stressed surface by DPC can only be detected at this edge of the crystal. At the opposite stressed surface, dissolution by DPC should be limited to the contact area to the piston. This contact area cannot be imaged with our experimental setup. Moreover, the accessible edge of the crystal atop the piston-contact area is insignificantly stressed and shows negligible elastic strain energy density.

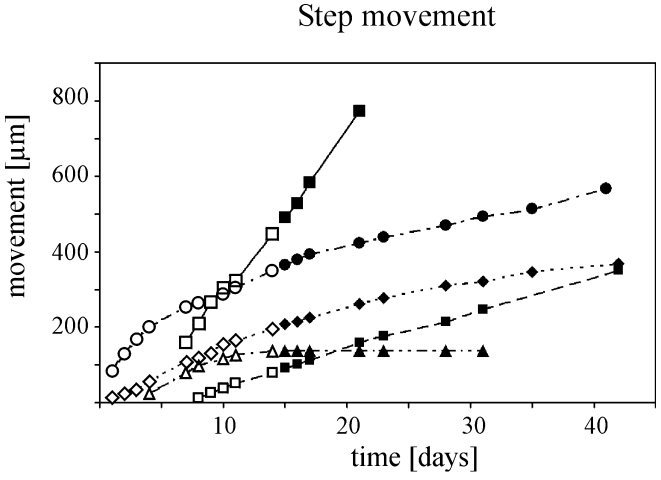

Fig. 6 Step advance induced by a temperature gradient of 0.006–0.01 K/mm during quasi-equilibrium (*open symbols*) and while applying inhomogeneous stress (*closed symbols*) according to the stress state A (Fig. 3). Although the applied stress should drive DPC, the step advance does not increase, in some cases it even decreases slightly

Figure 7a shows the free surface directly at the cell wall in the quasi-equilibrium state (exp. E 4.1). The distance between the edge of the crystal and the cell wall is in the range of the lateral optical resolution limit (~0.5 µm) or smaller. The dark speckled area at the right side in the topographic

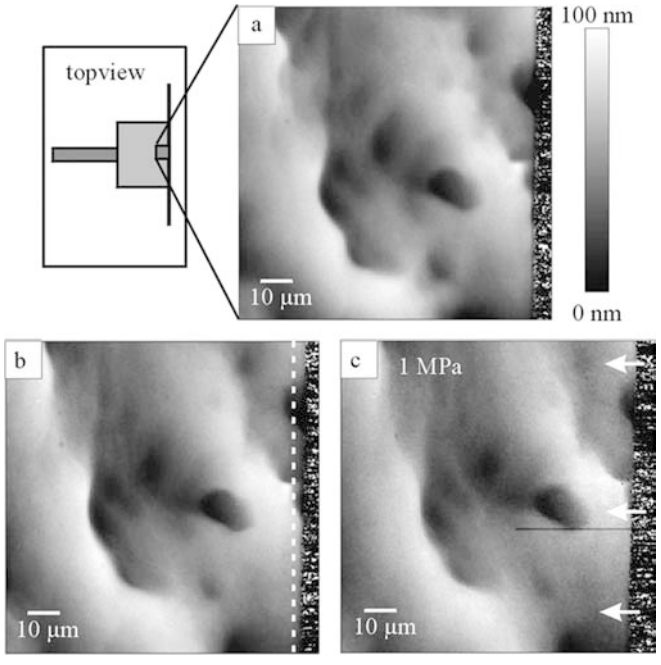

Fig. 7 a Halite (100) surface in a quasi-equilibrium state without applied stress. **b** The same surface area after 14 days without applied stress and at the instant when stress is applied for the first time. **c** The same surface area after 17 days with uniaxial stress of 1 MPa. The *black line* in **c** is an image artefact. The *dashed line* in **b** shows the rim position of the (100) surface in **c**. The *arrows* in **c** mark the direction of dissolution. The rim retreat velocity is 100 nm/day. The scale is valid for all images (**a**–**c**)

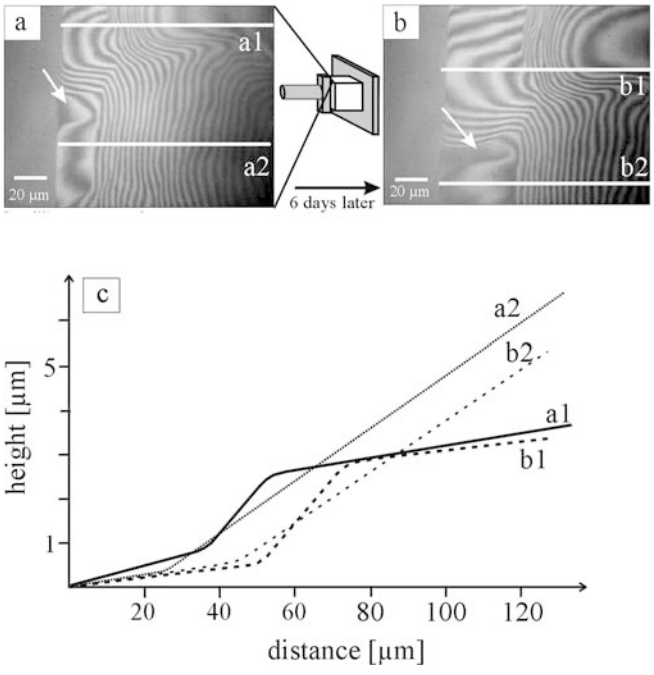

Fig. 8 Experiment with inhomogeneous elastic strain energy density (stress state B, Fig. 3). The profiles *a1*, *a2*, *b1* and *b2* from the interferograms **a** and **b** are shown in **c**. The displacement of the steps from the left to the right and the enlargement of the etch pit (see *arrows* in **a** and **b**) reflects progressive dissolution on the free surface of the crystal

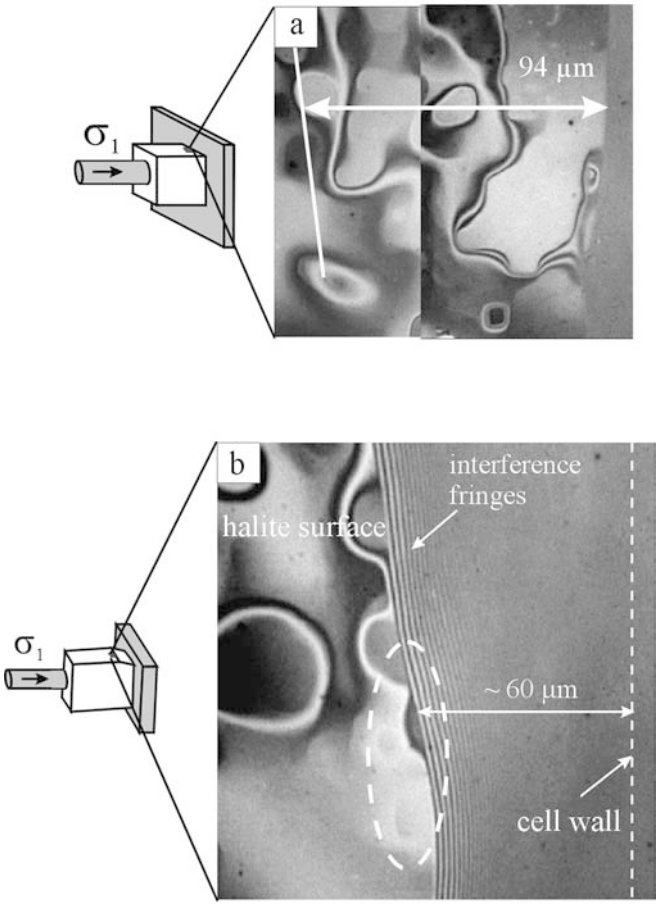

Fig. 10 The interferograms show the halite (100) surface area close to the cell wall in the quasi-open system. The interferogram **a** shows the surface at the beginning of the experimental run (E 7) and is composed of two individual images. The interferogram **b** shows the surface after 7 days at an applied stress of 0.4 MPa. The *white line* in **a** marks the rim position in **b**. Interference fringes are visible to the right of the rim at the halite edge indicating a facet inclined towards the cell wall. The estimated distance between the cell wall and the rim at the edge of the halite is ca. 60 µm

image represents an object that cannot be measured together with the free surface. This object can be either the cell wall or a strongly inclined surface area at the crystal edge. Figure 7b was taken immediately after stress had been applied to the crystal. The comparison of Fig. 7a and b reveals neither changes in surface morphology nor any retreat of the perpendicular oriented contact face. Figure 7c shows the same surface area under uniaxial stress (stress state A) 17 days later (exp. E 4.2). The two prominent pits visible in the middle and at the top-right of Fig. 7c are clearly closer to the dark area by approx. 1.7 µm than in Fig. 7b. As mentioned above, PSIM unfortunately does not allow one to precisely distinguish between the cell wall and strongly inclined facets at the crystal edge. Therefore, within the range of precision necessary in this case, we cannot distinguish between true convergence at the entire contact face or local dissolution

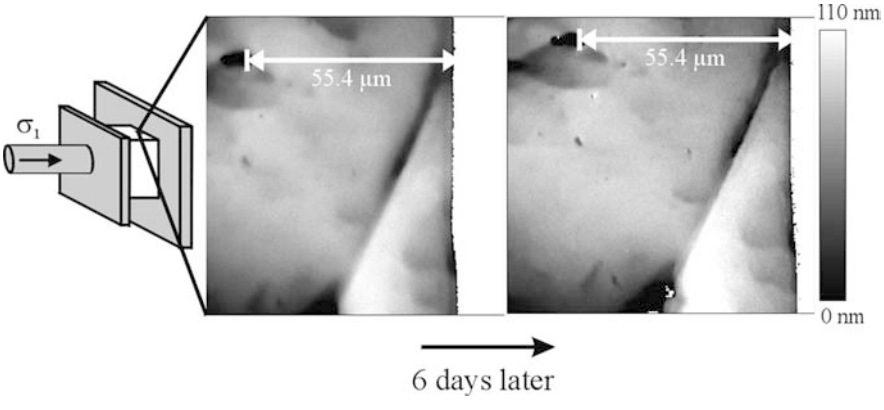

Fig. 9 The application of nearly homogeneous stress gives no change in the contact area halite-cell wall within 6 days

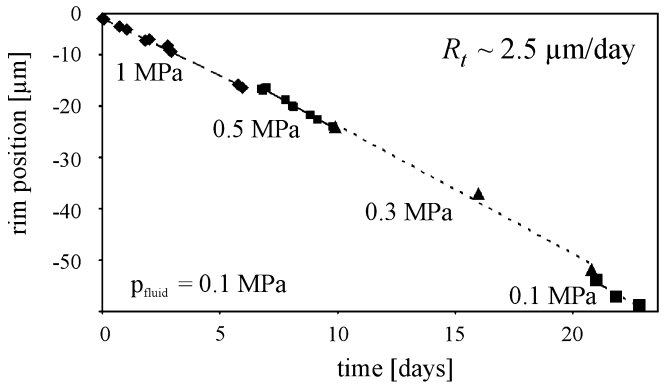

Fig. 11 Plot of the rim position on the free surface versus time in experiment E 6 with an inhomogeneous stress (stress state A) applied to the crystal in a quasi-open system. The retreat rate R_t is independent of the applied stress

at the crystal edge by the formation of strongly inclined facets, i. e., by retreat of the rim of the free surface. Regardless of edge dissolution or crystal convergence, quantitative evaluation of Fig. 7 yields a retreat velocity of approximately 100 nm/day (see arrows in Fig. 7c).

In order to evaluate the role of a high amount of elastic strain energy density and stress at the accessible free surface, experiment E 3 (Table 1) has been performed using stress state B (Fig. 3). The interferograms of Fig. 8a, b show a detail of the free surface next to the rectangular piston while stress is applied to the crystal. In Fig. 8c the profiles a1, a2, b1 and b2 from Fig. 8a, b are shown. It can be seen that the steps on the free surface of the crystal retreat and an etch-pit-like structure expands in size (see arrows in Fig. 8a, b)—clearly showing dissolution *on* the surface next to the piston. However, the left edge of the crystal (i.e., the rim of the free surface at the contact with the piston), where the observable surface ends, did not show any retreat or removal of material.

To study the effect of a near homogeneous state of stress combined with low elastic strain energy density, experiment E 5 (Table 1) was performed using stress state C (Fig. 3). In this setup the applied stress was 0.3 MPa. In Fig. 9, a surface area close to the cell wall is shown. Within six days of applied near homogeneous stress neither changes on the surface nor dissolution at the edge could be found.

Surface morphology in a quasi-open system

Experiments E 6 and E 7 (Table 1) were performed in a quasi-open system using stress state A. Figure 10 shows the interferograms of areas of the free surface close to the cell wall at the beginning (a) and at the end (b) of the experimental run E 7. During the experiments, the crystal dissolved continuously at the edge forming a retreating rim (see sketch in Fig. 10b), while the free surface did not show any growth or dissolution. The retreat rates of the rim in the experiments E 6 and E 7 were 2.5 and 13.5 µm/day, respectively. In Fig. 11, the rim position is plotted versus time for experiment E 6 with stress successively reduced in periods of several days. The data show that the rim retreat rate was *independent* of the applied stress and did even persist after the applied uniaxial stress had been taken off. As can be seen in Fig. 10b, extended dissolution at the crystal edge caused the interferometrically inaccessible surface area to increase in size. In the image a facet inclined towards the cell wall can be seen which was formed by the retreating rim. Although, as mentioned above, it is not possible to precisely locate the contact between the cell wall and the lower area of the inclined facet, it is still possible to determine this position within an accuracy of a few microns. For the experiment E 7 shown in Fig. 10b, the distance between cell wall and rim is about 60 µm. Comparison of this distance with the original distance of 94 µm (Fig. 10a) leads to a maximum convergence rate of ca. 7 µm/day. It should be noted that this kind of experiment requires at least some stress to avoid the opening of a gap between the crystal and the cell wall. In all experiments in the quasi-open system very small crystals of halite were formed outside of the cell, indicating transport of material out of the system.

Discussion

Our experiments reveal the fine-scale response of surface morphology to changes in thermodynamic conditions applied to a halite crystal in contact to aqueous solution. These experiments on halite, as a model material, can provide insights into some principal processes involved in the deformation of rocks by dissolution precipitation creep. In the following, we first discuss the effect of temperature observed in our experiments, then the effect of stress states, and finally the markedly different response in an open system compared to a closed system.

The solubility of NaCl in water depends on temperature. As shown in Fig. 4 changes in temperature can cause strong changes in the morphology of the halite surface in solution, if the volume ratio of liquid to solid is large. Here, the volume ratio of liquid to solid is approximately ten. Experiments without temperature control at room temperature do not cause significant alterations of the surface morphology within a few hours, reflecting the insignificant variations of room temperature within such a time frame. Nonetheless, in all other experiments presented here, temperature variations were further reduced by controlling the cell temperature at (30 ± 0.05) °C. Inevitably, the temperature difference between the interior and exterior of the cell and the presence of the optical window causes a temperature gradient in the cell, which leads to a noticeable effect in our experiments. The vertical temperature gradient of about 0.006–0.01 K/mm implies a temperature difference of up to 0.05 K between the bottom and the top of the crystal. The measured step kinematics of experiments E 2 and 4.1 on the colder surface gives a

deposition rate of 0.006 mm^3/day. Taking the solubility data from Farelo et al. (1993) and assuming a simple diffusion controlled transport model ($D_{NaCl} = 1.59\times10^{-9}$ m^2/s, Vitagliamo and Lyons 1956) with a cross-sectional area of 74 mm^2 along a diffusion path of 5 mm between top and bottom of the crystal, we obtain a mass transport equivalent of ca. 0.011 mm^3 solid NaCl per day, which is in reasonable agreement to the rate based on the measured step kinematics.

Application of inhomogeneous stress (stress state A, Fig. 3) in a closed system as shown in Fig. 7 causes a retreat rate at the edge of the surface of 100 nm/day. Assuming this retreat rate to be true convergence exclusively and assuming further that the material detached from the converging surfaces is deposited on all free surfaces equally, we would expect to see an advance of steps on the observed free surface when stress is applied. From a large number of micrographs taken on the entire free surface we estimated the total length of the growing steps on the 4×4 mm^2 surface to be between 17 and 35 mm. Taking this range of step length and the observed range of step heights, a convergence rate of 100 nm/day of both compressed surfaces with a total contact area of approx. 28 mm^2 should give rise to a step advance of 10–30 μm/day. In the quasi-equilibrium state, step advance rates up to 84 μm/day were measured (Fig. 6). Therefore, if the dissolution occurred across the whole area of the loaded faces by convergence, the advance rate should increase by up to 30 μm/day compared to quasi-equilibrium. Fig. 6 clearly gives no indication for an increased advance in this inferred magnitude when stress is applied. This indicates that the observed dissolution at the crystal edge may have contributions from a facet-like retreat which reduces the calculated amount of detached material and reduces the upper limit of the possible convergence rate.

Other single crystal experiments on DPC were reported by Hickman and Evans (1991, 1992, 1995), Röller et al. (1995), Martin et al. (1999) and Schutjens and Spiers (1999). The macroscopic experiments of Röller et al. (1995) and Martin et al. (1999) were performed on similarly sized crystals in contact with another crystal (halite, quartz or mica) and the piston. The stresses applied by these authors were between 0.1 and 2 MPa and an axial convergence was reported to be in the order of 0.1 to 2 μm/day. Their lower limit of 0.1 μm/day might be consistent with our results. Their upper limit of 2 μm/day is equivalent to the diffusive mass transport of 2.2×10^{-11} mol/s. This upper limit would correspond to an increase in step advance velocity in our experiment of 200 to 540 μm/day, depending on step height and total step length on the free surface. This discrepancy and the reported lack of correlation between convergence rate and magnitude of stress possibly point towards transport effects in a quasi-open system in the experiments of Röller et al. (1995) and Martin et al. (1999) as discussed below.

Hickman and Evans (1991, 1995) reported convergence rates of 10–50 nm/day using calotte-shaped crystals in contact with flat surfaces. This experimental setup is associated with large stress inhomogeneities at the loaded surfaces in contact with the solution. Thus, their experimental conditions better can be compared to our experiments with stress state B than to those with stress state A (Fig. 3). In experiment E 3 conducted according to stress state B (Fig. 3), we found no evidence for the retreat of the rim facing the piston, despite the applied stress of 1.9 MPa. In their experiments, Hickman and Evans (1991, 1995) applied loads of up to 14 MPa, which could have enhanced dissolution/reprecipitation rates due to rapid dissolution of plastically deformed zones of the material. Moreover, in the experiments of Hickman and Evans (1991, 1995) the shape of the capillary gap widening at the rim of the contact zone introduced gradients in capillary forces, which will further create driving forces for dissolution/reprecipitation. When inhomogeneous stress was applied in our experiment, we clearly observed dissolution on the free surface, while we observed no retreat or dissolution of the loaded contact area. In both types of experiments (stress states A and B), the inhomogeneous stress causes a significant inhomogeneity elastic or plastic strain energy density. Locally increased strain energy density causes a local increase of the solubility. Recently den Brok and Morel (2001) suggested that elastic strain energy fields are the origin of microstructural patterns forming on the free surfaces of stressed minerals in contact with aqueous solution. As Bathurst (1958) put it in other words: ''in any sediment made of grains and water each crystal lattice (grain) is always elastically strained in the vicinity of an intergranular boundary and this strain is enormously increased by the weight of an overburden''. This implies an increased local solubility at these point contacts. Our experiments with inhomogeneously stressed crystals show that the crystals always dissolve at the sites with increased elastic or plastic strain energy density. Nominally homogeneous elastic strain according to stress state C has not caused any visible effects in our experiments, neither growth nor dissolution. Bos et al. (2000) have presented the microstructural results of experiments on poly-phase aggregates, where mixtures of halite and kaolinite in NaCl solution were exposed to continuous shear-deformation. With sliding velocities of up to 10 μm per second (ca. 10^8 nm per day) they built up overall macroscopic shear stresses of up to 8 MPa. At point contacts in aggregates the stress can exceed the macroscopic value by far. We suspect that in this way local plastic deformation and cataclasis was forced, and the local build-up of internal energy was relaxed by rapid dissolution of the deformed zones and subsequent reprecipitation. These experiments clearly proved that such wet aggregates deform by DPC rather than by dislocation creep. In our experiments, the strain rates were at least 10^5 times lower than in the experiments of Bos et al. (2000).

The observed shape evolution of a single crystal during a day varies from the nanometer range in a closed system to the micron range in a quasi-open system. De Meer and Spiers (1997) reported that the rate of compaction creep of wet gypsum with through-flowing solution in an open-system is increased by a factor of 10 to 30 compared to experiments in a closed system. They concluded that precipitation was the rate-controlling step. In our experiments E 6 and E 7, the independence of the dissolution rate on the applied stress, as also observed by Martin et al. (1999), indicates that the dissolution of the crystal in the quasi-open system is not governed alone by stress, but by transport of NaCl out of the cell. In accordance with the results of de Meer and Spiers (1997), this could mean that a quasi-open system can promote DPC processes. Notably, a marked volumetric strain has been recognised for natural rocks deformed by dissolution precipitation creep (e.g., Ring and Brandon 1999), implying an open system. In the case of net dissolution of material and transport out of the system, the orientation of the principle stress axes will control the orientiation of the (finite) strain axes and the microfabric of the rock deformed by DPC.

Conclusions

Most previous studies suppose that rock deformation by DPC can proceed in a closed system and is exclusively driven by a homogeneous stress field on the grain scale. In this scenario, diffusional transport is caused by purely deviatoric stress-induced chemical potential gradients, supposedly related to the different orientation of interfaces with respect to the principle stress axes. However, in our high-resolution experiments, we obtained the least shape evolution—if any—when the crystal was exclusively subject to practically homogeneous uniaxial stress. We found that additional factors causing local or temporal variations in solubility enhance DPC. In our experiments the significance of factors promoting DPC can be ranked as follows. First, the disturbance of equilibrium by changes in extensive parameters such as temperature has the most pronounced effect of all, and even small temperature gradients (0.01 K/mm in our experiment) give rise to significant continuous DPC on the laboratory time scale. Second, the migration of super- or undersaturated fluids in an open system is effectively promoting DPC. Third, small but measurable morphological changes are caused by gradients in elastic (or plastic) strain energy density as caused by point contacts.

Thus it appears that DPC in nature is promoted by reasons other than just pure homogeneous stress. Our findings suggest that open systems with percolation of fluids through the rock, e.g., by fluid flow along gradients in temperature or across compositional boundaries, or by episodic changes of extensive parameters affecting solubility, in particular pore fluid pressure, could be prerequisite for rapid deformation by DPC. As such, on geological time scales, solubility variations caused by pore pressure fluctuations related to seismicity, or even to Earth tides, may provide an appropriate acceleration mechanism. In sediments with a large pore volume, point-like grain contacts inducing gradients in elastic strain energy on the grain scale are the rule rather than the exception, and they will enhance DPC during compaction. DPC may be least efficient in a purely homogeneous stressed and closed system with transport restricted to the grain scale.

Acknowledgements We thank G. Andersen, W. Schrimpf, J. Schiller and F. Heinke for technical support. Financial support from the Deutsche Forschungsgemeinschaft (Sonderforschungsbereich 526) is gratefully acknowledged. Editorial handling by J. Hoefs and helpful reviews by J. Urai and an anonymous reviewer are gratefully appreciated.

References

Astilleros JM, Pina CM, Fernandez-Diaz L, Putnis A (2000) The effect of barium on calcite (104) surfaces during growth. Geochim Cosmochim Acta 64:2965–2972

Aziz DJ (1998) Interferometric measurement of surface roughness in engine cylinder walls. Opt Eng 37:1429–1434

Bos B, Peach CJ, Spiers CJ (2000) Frictional-viscous flow of simulated fault gouge caused by the combined effects of phyllosilicates and pressure solution. Tectonophysics 327:173–194

Bos B, Spiers CJ (2002) Frictional-viscous flow of phyllosilicate-bearing fault rock: microphysical model and implications for crustal strength profiles. J Geophys Res 107, B2: art no 2028

Bruning JH, Herriott DR, Gallagher JE, Rosenfeld DP, White AD, Brangaccio DJ (1974) Digital wavefront measuring interferometer for testing optical surfaces and lenses. Appl Opt 13(11):2693–2703

de Meer S, Spiers CJ (1997) Uniaxial compaction creep of wet gypsum aggregates. J Geophys Res 102(B1):875–891

de Meer S, Spiers CJ, Peach CJ, Watanabe T (2002) Diffusive properties of fluid-filled grain boundaries measured electrically during active pressure solution. Earth Planet Sci Lett 200:147–157

den Brok SWJ, Zahid M, Passchier CW (1999a) Pressure solution compaction of sodium chlorate and implications for pressure solution in NaCl. Tectonophysics 307:297–312

den Brok SWJ, Zahid M, Passchier CW (1999b) Stress-induced grain boundary migration in very soluble brittle salt. J Struct Geol 21:147–151

den Brok SWJ, Morel J (2001) The effect of elastic strain on the microstructure of free surfaces of stressed minerals in contact with an aqueous solution. Geophys Res Lett 28, 4:603–606

Derjaguin BV, Churaev NV, Muller VM (1987) Surface forces. Consultants Bureau, New York, XIX, 440 pp

Durney DW (1976) Pressure-solution and crystallization deformation. Philos Trans R Soc Lond A 283:229–240

Elliott D (1973) Diffusion flow laws in metamorphic rocks. Bull Geol Soc Am 84:2645–2664

Farelo F, von Brachel G, Offermann H (1993) Solid-liquid equilibria in the ternary system NaCl-KCl-H_2O. Can J Chem Eng 71:141–146

Gibbs JW (1906) On the equilibrium of heterogeneous substances. In: The collected works of J. Willard Gibbs, vol 1. Yale Univ Press, New Haven, pp 184–201

Gratier JP (1993) Experimental pressure solution of Halite by an indenter technique. Geophys Res Lett 20, 15:1647–1650

Groshong RHJ (1988) Low temperature deformation mechanisms and their interpretation. Bull Geol Soc Am 100:1329–1360

Hart M, Vass DG, Begbie ML (1998) Fast surface profiling by spectral analysis of white-light interferograms with Fourier transform spectroscopy. Appl Opt 37:1764–1769
Heald MT (1956) Cementation of Simpson and St. Peter Sandstones in parts of Oklahoma, Arkansas and Missouri. J Geol 64:16–30
Heidug WK (1995) Intergranular solid-fluid phase transformations under stress: The effect of surface forces. J Geophys Res 100, B4:5931–5940
Hickman SH, Evans B (1991) Experimental pressure solution in halite: the effect of grain/interphase boundary structure. J Geol Soc Lond 148:549–560
Hickman SH, Evans B (1992) Growth of grain contacts in halite by solution-transfer: implications for diagenesis, lithification and strength recovery. In: Evans B, Wong TF (eds) Fault mechanics and transport properties of rocks, Academic Press, New York, pp 253–280
Hickman SH, Evans B (1995) Kinetics of pressure solution at halite-silica interfaces and intergranular clay films. J Geophys Res 100, B7:13113–13132
Hirth G, Kohlstedt DL (1995) Experimental constraints on the dynamics of the partially molten upper-mantle. 1. deformation in the diffusion creep regime. J Geophys Res Solid Earth 100:1981–2001
Jones CE, Unwin PR, Macpherson JV (2003) In situ observation of the surface processes involved in dissolution from the cleavage surface of calcite in aqueous solution using combined scanning electrochemical ±atomic force microscopy (SECM-AFM). Chemphyschem 4:139–146
Jordan G, Higgins SR, Eggleston CM, Knauss KG, Schmahl WW (2001) Dissolution kinetics of magnesite in acidic aqueous solution, a hydrothermal atomic force microscopy (HAFM) study: Step orientation and kink dynamics. Geochim Cosmochim Acta 65:4257–4266
Kamb WB (1961) The thermodynamic theory of nonhydrostatically stressed solids. J Geophys Res 66, 1:259–271
Knipe RJ (1989) Deformation mechanisms—recognition from natural tectonites. J Struct Geol 11:127–146
Lehner FK (1990) Thermodynamics of rock deformation by pressure solution. In: Barber DJ, Meredith PD (eds) Deformation processes in minerals, ceramics and rocks, Unwin Hyman, London, pp 296–333
Lehner FK (1995) A model for intergranular pressure solution in open systems. Tectonophysics 245:153–170
Lehner FK, Bataille J (1984/85) Nonequilibrium thermodynamics of pressure solution. Pure Appl Geophys 122:53–85
Leroy YM, Heidug WK (1994) Geometrical evolution of stressed and curved solid-fluid phase boundaries. 2. Stability of cylindrical pores, J Geophys Res 99(B1):517–530
Linnik W (1933) Ein Apparat für mikroskopische-interferometrische Untersuchung reflektierender Objekte (Mikrointerferometer). C R Acad Sci URSS 1:18–23
Lüttge A, Bolton EW, Lasaga AC (1999) An interferometric study of the dissolution kinetics of anorthite: the role of reactive surface area. Am J Sci 299, 7–9:652–678
Lüttge A, Winkler U, Lasaga AC (2003) Interferometric study of the dolomite dissolution: a new conceptual model for mineral dissolution. Geochim Cosmochim Acta 67:1099–1116
MacInnis IN, Brantley SL (1993) Development of etch pit size distributions on dissolving minerals. Chem Geol 105:31–49
Martin B, Röller K, Stöckhert B (1999) Low-stress pressure solution experiments on halite single-crystals. Tectonophysics 308:299–310
McClay KR (1977) Pressure solution and Coble creep in rocks and minerals: a review. J Geol Soc Lond 134:57–70
Mirau A (1955) Méthodes et appareils français de mesure du fini des surfaces. Rev Univers Mines 11:461–469
Morel J, den Brok SWJ (2001) Increase in dissolution rate of sodium chlorate induced by elastic strain. J Cryst Growth 222:637–644
Onuma K, Tsukamoto K, Nakadate S (1993) Application of real time phase shift interferometer to the measurement of concentration field. J Cryst Growth 129:706–718
Onuma K, Kameyama T, Tsukamoto K (1994) In situ study of surface phenomena by real time phase shift interferometry. J Cryst Growth 137:610–622
Ostapenko GT (1968) Recrystallization of minerals under stress. Geochem Int 5:183–186
Paterson MS (1973) Nonhydrostatic thermodynamics and its geologic applications. Rev Geophys Space Phys 11(2):355–389
Peskleway CD, Henderson GS, Wicks FJ (2003) Dissolution of gibbsite: direct observations using fluid cell atomic force microscopy. Am Miner 88:18–26
Raj R, Chyung CK (1981) Solution-precipitation creep in glass ceramics. Acta Metall 29:159–166
Renard F, Dysthe D, Feder J, Bjorlykke K, Jamtveit B (2001) Enhanced pressure solution creep rates induced by clay particles: experimental evidence in salt aggregates. Geophys Res Lett 28:1295–1298
Renard F, Gratier JP, Jamtveit B (2000) Kinetics of crack-sealing, intergranular pressure solution, and compaction around active faults. J Struct Geol 22:1395–1407
Ring U, Brandon MT (1999) Ductile deformation and mass loss in the Franciscan subduction complex: implications for exhumation processes in accretionary wedges. In: Ring U, Brandon MT, Lister GS, Willett SD (eds) Exhumation processes: normal faulting, ductile flow, and erosion. Geol Soc Lond Spec Publ 154:55–86
Röller K, Martin B, Stöckhert B (1995) Experimental studies on pressure solution along special interfaces. Bochumer Geol Geotech Arb 44:173–177
Rosenberg CL (2001) Deformation of partially molten granite: a review and comparison of experimental and natural case studies. Int J Earth Sci 90:60–76
Rutter EH (1976) The kinetics of rock deformation by pressure solution. Philos Trans R Soc Lond A 283:203–219
Rutter EH (1983) Pressure solution in nature, theory and experiment. J Geol Soc Lond 140:725–740
Sandoz P (1996) An algorithm for profilometry by white-light phase-shifting interferometry. J Mod Optics 43:1545–154
Schutjens PMTM, Spiers CJ (1999) Intergranular pressure solution in NaCl: Grain-to-grain contact experiments under the optical microscope. Oil Gas Sci Technol Rev IFP 54, 6:729–750
Schwarz S, Stöckhert B (1996) Pressure solution in siliclastic HP-LT metamorphic rocks—constraints on the state of stress in deep levels of accretionary complexes. Tectonophysics 255:203–209
Shimizu I (1995) Kinetics of pressure solution creep in quartz: theoretical considerations. Tectonophysics 245:121–134
Sorby HC (1863a) Über Kalkstein-Geschiebe mit Eindrücken. N Jahrb Min Geol Palaeontol: 801–807
Sorby HC (1863b) On the direct correlation of mechanical and chemical forces. Proc R Soc Lond 12:538–550
Sorby HC (1865) On impressed limestone pebbles, as illustrating a new principle in chemical geology. Proc West Yorks Geol Soc 14:458–461
Spiers CJ, Schutjens PMTM (1990) Densification of crystalline aggregates by fluid-phase diffusional creep. In: Barber DJ, Meredith PG (eds) Deformation processes in minerals, ceramics and rocks, Unwin Hyman, London, 334–353
Spiers CJ, Schutjens PMTM, Brzesowsky RH, Peach CJ, Liezenberg JL, Zwart HJ (1990) Experimental determination of constitutive parameters governing creep of rocksalt by pressure solution. In: Knipe RJ, Rutter EH (eds) Deformation mechanisms, rheology and tectonics. Geol Soc Spec Publ Lond 54:215–227
Spiers CJ, Brzesowsky RH (1993) Densification behaviour of wet granular salt: Theory versus experiment, In: Seventh Symposium on Salt, vol 1. Elsevier, Amsterdam, pp 83–92

Stöckhert B, Wachmann M, Küster M, Bimmermann S (1999) Low effective viscosity during high pressure metamorphism due to dissolution precipitation creep: the record of HP-LT metamorphic carbonates and siliciclastic rocks from Crete. Tectonophysics 303:299–319

Tada R, Siever R (1986) Experimental knife-edge pressure solution of halite. Geochim Cosmochim Acta 50:29–36

Teng HH, Fenter P, Cheng L, Sturchio NC (2001) Resolving orthoclase dissolution processes with atomic force microscopy and X-ray reflectivity. Geochim Cosmochim Acta 65:3459–3474

Urai JL, Spiers CJ, Zwart HJ, Lister GS (1986) Weakening of rock salt by water during long-term creep. Nature 324:554–557

Vitagliamo V, Lyons PA (1956) Diffusion coefficients for aqueous solutions of sodium chloride and barium chloride. J Am Chem Soc 78:1549–1552

Weyl PK (1959) Pressure solution and the force of crystallisation—A phenomenological theory. J Geophys Res 64(11):2001–2025

Wimmer FT, Kobes W, Fine ME (1963) Tensile properties of NaCl-BaNr solid solution single crystals. J Appl Phys 34(6:)1775–1778